Proceedings of International Conference on Heat Exchanger Fouling and Cleaning VIII - 2009 (Peer-reviewed)
June 14-19, 2009, Schladming, Austria
Editors: H. Müller-Steinhagen, M.R. Malayeri and A.P. Watkinson

DEPOSITION MODELING FROM MULTI-PHASE DISPERSED FLOW – A BOUNDARY LAYER WALL FUNCTION APPROACH

S.G. Johnsen[1] **and S.T. Johansen**

[1] SINTEF Materials and Chemistry, N-7465 TRONDHEIM, Norway, E-mail (sverre.g.johnsen@sintef.no):

ABSTRACT

Modeling of mass transfer of particles to solid surfaces is a considerable challenge in most industrial processes, including heat exchanger applications. Using computational fluid dynamics (CFD) directly on these applications is extremely time consuming as we need an extremely fine grid to capture the details of the complex physical processes that dominate in the near-wall region.

We propose a detailed boundary layer model, which can couple the physics in the wall region with the external flow. The developed mass-transfer wall function can be applied as a boundary condition for coarse grid CFD models. The boundary layer model incorporates gravity, turbulence and hydrodynamic lift and drag. In addition we include the effects of Brownian diffusion, thermophoresis, extended DLVO forces and the inter-particle collisions. Heat transfer, by the liquid and particulate phases, is coupled to the momentum equations.

The one-dimensional boundary layer model is solved numerically in a fine grid that is capable of resolving the near wall XDLVO force length scales.

When dispersed phase particles touch the wall they are considered deposited and removed from the flow. The effect of adhesion probability and particle re-entrainment is not considered.

Thermodynamic and chemical effects, such as phase change or precipitation, are not included in this work.

INTRODUCTION

Fouling of solid surfaces exposed to fluids carrying particles, is a common and much investigated problem. Fouling is defined as accumulation of unwanted material on solid surfaces. The topic is of general interest in most process industries, including oil/gas, minerals, metals, cement, food, marine and fishing, and also areas like medicine and environment. Consequently, a vast amount of work has been done in this field. Sippola and Nazaroff (2002) and Guha (2008) cite an extensive list of published studies. They give comprehensive reviews of transport and deposition mechanisms of particles in gas and liquid flows, but neither of them includes near-wall XDLVO forces or granular stress effects. Johansen (1991a) describes the deposition of particles from a gas flow. Combined thermal-turbulent deposition was first time predicted by Johansen (1991b) (for gases) and for liquids by Adomeit and Renz (1996).

In this paper, we develop a mathematical framework for solving the Navier-Stokes equations inside the boundary layer close to a solid surface, for a liquid phase carrying a dispersed particle phase. By numerical solution of the proposed transport equations for particle volume fraction, temperature and axial liquid velocity, we obtain the deposition mass transfer coefficient. The resulting mass transfer coefficient can be employed as a wall function for coarse grid CFD simulations. Our model includes the hydrodynamic forces, drag and lift, thermophoresis, turbulence, granular stress effects and near-wall XDLVO forces.

First, we give a detailed overview of the model. Next, we employ the developed model to study how the deposition flux is affected by the different physical mechanisms involved, for different particle sizes.

GOVERNING EQUATIONS

We consider an Eulerian-Eulerian two-fluid model, consisting of an incompressible continuous liquid (*l*) phase and a mono-disperse incompressible inert particulate (*p*) phase ($CaCO_3$), flowing close to a hot steel wall, as illustrated in Fig. 1. For simplicity, we will most of the time omit the *p* index when addressing particle properties. It is furthermore assumed steady turbulent flow, where the model

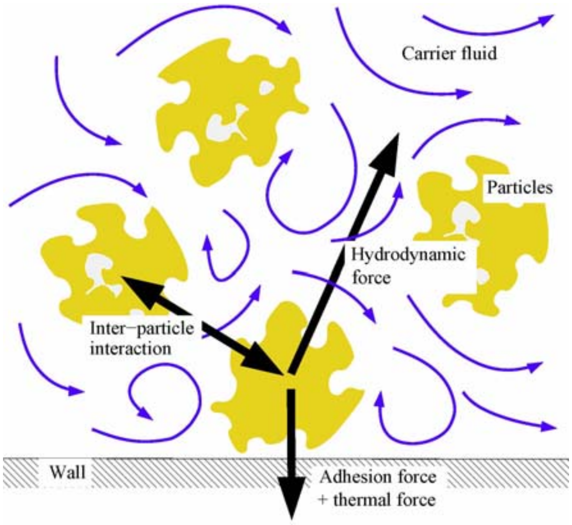

Fig. 1 Schematic of the flow of a cold suspension close to a hot wall. The particles are affected by hydrostatic forces, inter particle interactions, thermal and particle-wall forces.

equations can be derived from volume and ensemble averaged Navier-Stokes equations coupled with heat transport equations. *Bulk* indicates the conditions just outside the boundary layer. We do not consider thermodynamic effects, so particle generation or phase transitions do not occur.

Averaging Procedures and Notation

The conservation equations are derived by volume averaging over some arbitrary control volume, in order to handle the unknown distribution of the constituents inside the volume. Via the volume averaging method, we may treat the dispersed phase as a continuous phase, and we may apply the well-known conservation equations of continuum mechanics. The details on volume averaging may be found in classical textbooks on multiphase flow, such as (Crowe et al., 1997; Soo, 1989). Moreover, the conservation equations are ensemble averaged. All quantities are thus understood as volume and ensemble averages, with no further notice. Some of the terms, however, are not written out explicitly, and these terms are enclosed by brackets, < >, denoting an ensemble average of the complete term. Finally, when introducing turbulence, there will be yet another layer of ensemble averaging, to handle the influence on the particles by the stochastic turbulent fluctuations, denoted by $''$, of the liquid properties.

Stress terms, such as granular, thermal or Reynolds stresses, originate from the correlations between fluctuating properties. We neglect, however, for simplicity, correlation terms of order three or more, such as $\left\langle \alpha'' v'' v'' \right\rangle$.

Conservation Equations

Without turbulence, the particle phase continuity equation is

$$\vec{\nabla}(\rho_p \alpha_p \vec{\boldsymbol{v}}) = 0 \quad , \tag{1}$$

and the liquid and particulate momentum equations are

$$\vec{\nabla}\left(\alpha_l \rho_l \vec{\boldsymbol{u}}\vec{\boldsymbol{u}}\right) = \\ - \underbrace{\alpha_l \vec{\nabla} P}_{\text{Pressure gradient}} + \underbrace{\alpha_l \vec{\nabla} \boldsymbol{\tau}_l}_{\text{Viscous stress}} + \underbrace{\alpha_l \rho_l \vec{\boldsymbol{g}}}_{\text{External fields}} + \underbrace{\vec{\boldsymbol{f}}_{p,l}}_{\substack{\text{Particle-liquid}\\ \text{interactions}}} \quad , \tag{2}$$

and

$$\vec{\nabla}\left\langle \alpha_p \rho_p \vec{\boldsymbol{v}}\vec{\boldsymbol{v}} \right\rangle = \\ - \underbrace{\alpha_p \vec{\nabla} P}_{\text{Pressure gradient}} + \underbrace{\alpha_p \vec{\nabla} \boldsymbol{\tau}_l}_{\text{Viscous stress}} + \underbrace{\alpha_p \rho_p \vec{\boldsymbol{g}}}_{\text{External fields}} - \underbrace{\vec{\boldsymbol{f}}_{p,l}}_{\substack{\text{Particle-liquid}\\ \text{interaction}}} + \underbrace{\vec{\boldsymbol{f}}_p^{XDLVO}}_{\text{Near wall force}} \quad , \tag{3}$$

where the liquid-particle interaction force is given by

$$\vec{\boldsymbol{f}}_{p,l} = \underbrace{\frac{\alpha_p \rho_p}{t_p}\left(\vec{\boldsymbol{v}} - \vec{\boldsymbol{u}}\right)}_{\text{Drag force}} + \underbrace{\alpha_p \rho_p C_{L,p}\left(\vec{\boldsymbol{v}} - \vec{\boldsymbol{u}}\right) \times \left(\vec{\nabla} \times \vec{\boldsymbol{u}}\right)}_{\text{Lift force}} + \underbrace{\left\langle \alpha_p \vec{\boldsymbol{f}}_p^{T} \right\rangle}_{\substack{\text{Thermal}\\ \text{force}}} \quad . \tag{4}$$

The added mass and Basset forces are currently neglected. As can be seen, we have retained the brackets enclosing the convective term on the left and the thermal force contribution on the right hand side of Eq. (3). These terms will be developed below.

In general, the bulk flow and the wall have different temperatures, so there will be a transport of heat between the two, and a thermal boundary layer will exist. The heat will be transported by the fluid and the particles. In general, there will also be a temperature difference between the particles and the fluid. The stationary y-directional heat transport equations for the liquid and particle phases are

$$\underbrace{\frac{\partial\left(\alpha_l \rho_l C_{p,l} u_y T_l\right)}{\partial y}}_{\text{Convection}} = \frac{\partial}{\partial y}\underbrace{\left[\alpha_l k_{h,l} \frac{\partial T_l}{\partial y}\right]}_{\text{Conduction}} + \underbrace{\frac{3\alpha_p h_{p,l}}{4 d_p}\left(T_p - T_l\right)}_{\text{Particle-liquid heat exchange}} \quad , \tag{5}$$

$$\frac{\partial}{\partial y}\left(\underbrace{\alpha_p \rho_p C_{p,p} v_y T_p}_{\text{Convective heat transport}} - \underbrace{\frac{\alpha_p \rho_p v_g C_{p,p}}{\mathrm{Pr}_{g,p}} \frac{\partial T_p}{\partial y}}_{\text{Collisional heat exchange}} \right) = - \underbrace{\frac{3\alpha_p h_{p,l}}{4 d_p}\left(T_p - T_l\right)}_{\text{Particle-liquid heat exchange}} \quad , \tag{6}$$

where we have assumed near-ideal behavior, with constant specific heat capacities such that the enthalpy may be expressed as $C_p T$, and homogeneous particle temperatures.

Momentum contributions

In this section we discuss the momentum contributions entering the particle momentum equation, Eq. (3). The external field term contains body forces such as gravity and electrostatic forces. We consider vertical flow only, and we do not consider electrical forces, although the mirror charge force acting upon charged particles close to an electrically conducting wall may be significant. The particle-liquid interaction terms are hydrodynamic drag and lift and thermal interactions. Below we elaborate on the XDLVO, lift, thermal and convective terms of Eq. (3). The drag force is modeled by Stokes' law, $t_p = \rho d^2 / 18 \mu_l$, restricting the upper limit particle diameter to approximately $10 \mu m$.

XDLVO forces. The force contributions from the extended DLVO theory include the Lifshitz-van der Waals force (LW), the electrostatic double-layer force (EL), and the acid-base force (AB), based on the model developments of Hoek and Agarwal (2006) and van Oss (2006), such that

$$\vec{\boldsymbol{F}}^{XDLVO} = \vec{\boldsymbol{F}}^{LW} + \vec{\boldsymbol{F}}^{EL} + \vec{\boldsymbol{F}}^{AB} \quad , \tag{7}$$

where the LW contribution is $\vec{\boldsymbol{F}}^{LW} = A_H d / 12 h^2 \, \hat{\mathbf{e}}_{\mathrm{y}}$, the EL contribution is $\vec{\boldsymbol{F}}^{EL} = \frac{\pi \varepsilon_l d \kappa \, \mathrm{e}^{-\kappa h}}{2}\left[\frac{\left(\zeta_p + \zeta_w\right)^2}{1 + \mathrm{e}^{-\kappa h}} - \frac{\left(\zeta_p - \zeta_w\right)^2}{1 - \mathrm{e}^{-\kappa h}}\right] \hat{\mathbf{e}}_{\mathrm{y}}$, and the AB contribution is $\vec{\boldsymbol{F}}^{AB} = \pi d \cdot \Delta G_{h_0}^{AB} \, \mathrm{e}^{(h_0 - h)/\lambda} \, \hat{\mathbf{e}}_{\mathrm{y}}$. The Hamaker

Table 1 XDLVO parameters for $CaCO_3$ particles and a steel surface submerged in water, as reported by Ojaniemi et al. (2008), but corrected in accordance with personal communication with Ojaniemi.

γ^{LW}_{l}	2.18E-02	J/m^2
γ^{LW}_{w}	4.28E-02	J/m^2
γ^{LW}_{p}	2.67E-02	J/m^2
γ^{+}_{l}	2.55E-02	J/m^2
γ^{-}_{l}	2.55E-02	J/m^2
γ^{+}_{w}	2.00E-03	J/m^2
γ^{-}_{w}	1.15E-02	J/m^2
γ^{+}_{p}	2.00E-03	J/m^2
γ^{-}_{p}	2.84E-02	J/m^2
$\varepsilon_{r,l}$	66	
ζ_w	-3.00E-02	V
ζ_p	-4.00E-02	V
λ	4.00E-10	m

constant is given by $A_H = -24\pi h_0^2\left(\sqrt{\gamma_l^{LW}} - \sqrt{\gamma_w^{LW}}\right)\left(\sqrt{\gamma_p^{LW}} - \sqrt{\gamma_l^{LW}}\right)$, the inverse Debye screening length is given by $\kappa = \sqrt{(2F_a^2 I)/(\varepsilon_l RT)}$, and

$$\Delta G_{h_0}^{AB} = 2\Big[\sqrt{\gamma_l^+}\left(\sqrt{\gamma_w^-} + \sqrt{\gamma_p^-} - \sqrt{\gamma_l^-}\right) + \sqrt{\gamma_l^-}\left(\sqrt{\gamma_w^+} + \sqrt{\gamma_p^+} - \sqrt{\gamma_l^+}\right) - \left(\sqrt{\gamma_w^+\gamma_p^-} + \sqrt{\gamma_w^-\gamma_p^+}\right)\Big].$$

Here, we consider XDLVO forces between the particles and the wall. We neglect inter-particle XDLVO forces, such that there are neither repulsive nor adhesive forces between the particles, and no flocculation will occur. These contributions may, however, be of importance in some industrial applications. We apply numeric values for the XDLVO parameters, as employed by Ojaniemi et al. (2008), presented in Table 1. Depending on the particle and wall roughness, the XDLVO theory is not applicable to large particles. Due to the limited effect of the XDLVO forces on large particle deposition rates, so no upper particle size limit has been imposed on the XDLVO model.

Lift forces. We neglect the effects of liquid vorticity and particle rotations, so there is no Magnus force contribution. The Eq. (4) Saffman lift force is expressed by, (Johansen, 1991a),

$$\overline{\boldsymbol{f}}^{Saff} = -\frac{3.08\alpha\sqrt{\mu_l \rho_l}}{d}\sqrt{\left|\frac{\partial u_x}{\partial y}\right|}\left(v_x - u_x\right)\mathbf{e}_y \ , \qquad (8)$$

where it is assumed that the axial gradient of the y-directional fluid velocity is negligible.

Thermal forces. When the fluid and the wall have different temperatures, such that a temperature gradient is established normal to the wall, this adds to the deposition mechanism. Both hot and cold walls may give precipitation of particles, due to temperature dependent solubility. In addition thermophoresis will, generally, drive particles towards cold walls and away from hot walls.

The thermal force in Eq. (3) is split into two parts, a random contribution due to thermal fluctuations, and a thermophoretic (Soret) contribution,

$$\left\langle \alpha \overline{\boldsymbol{f}}^{T} \right\rangle = \left\langle \alpha^R \overline{\boldsymbol{f}}^{T,R} \right\rangle + \alpha \left\langle \overline{\boldsymbol{f}}^{T,S} \right\rangle \ . \qquad (9)$$

The Soret contribution is modeled by, (McNab and Meisen, 1973),

$$\left\langle \overline{\boldsymbol{f}}^{T,S} \right\rangle = -\frac{\beta_T \mu_l}{t_p} \overline{\nabla} \ln T \ , \qquad (10)$$

where the thermophoretic force strength is given by $\beta_T = 0.26 k_{h,l} / \left(k_{h,p} + 2k_{h,l}\right)$. The random contribution gives a force that averages to zero, but the force generates thermal particle velocities which will enter through the left-hand-side convective term of Eq. (3), as described below.

The convective term. We consider the particle velocity on three different scales, macro (average velocity), meso (granular), and micro (thermal) scales. The source of the granular velocity is the inter-particle collisions that occur in dense suspensions, while the thermal velocity is due to collisions with the thermally agitated liquid molecules. Adopting the simplifying assumption that there is no correlation between scales, $\left\langle \vec{\boldsymbol{v}} \right\rangle \left\langle \alpha\rho \vec{\boldsymbol{v}}^G \right\rangle = \left\langle \vec{\boldsymbol{v}} \right\rangle \left\langle \alpha\rho \vec{\boldsymbol{v}}^T \right\rangle = \left\langle \alpha\rho \vec{\boldsymbol{v}}^G \vec{\boldsymbol{v}}^T \right\rangle = 0$, so $\vec{\boldsymbol{v}} = \left\langle \vec{\boldsymbol{v}} \right\rangle + \vec{\boldsymbol{v}}^G + \vec{\boldsymbol{v}}^T$, the left-hand-side convective term of Eq. (3) becomes

$$\overline{\nabla}\left\langle \alpha\rho \vec{\boldsymbol{v}}\vec{\boldsymbol{v}} \right\rangle \rightarrow \overline{\nabla}\left\{ \alpha\rho \left\langle \vec{\boldsymbol{v}} \right\rangle \left\langle \vec{\boldsymbol{v}} \right\rangle + \left\langle \alpha\rho \vec{\boldsymbol{v}}^G \vec{\boldsymbol{v}}^G \right\rangle + \left\langle \alpha\rho \vec{\boldsymbol{v}}^T \vec{\boldsymbol{v}}^T \right\rangle \right\} \ , \qquad (11)$$

where $\left\langle \vec{\boldsymbol{v}} \right\rangle$ is the ensemble averaged velocity vector, and $\vec{\boldsymbol{v}}^G$ and $\vec{\boldsymbol{v}}^T$ contains the deviatory components caused by particle collisions and thermal fluctuations, respectively.

Assuming that the particles are in thermal equilibrium with the liquid and applying the principle of equipartition of the energy, the thermal stress term of Eq. (11) becomes

$$\left\langle \alpha\rho \vec{\boldsymbol{v}}^T \vec{\boldsymbol{v}}^T \right\rangle \approx \alpha\rho \frac{k_B T}{m} \mathbf{I} \ . \qquad (12)$$

The granular stress term of Eq. (11) is modeled, in accordance with (Gidaspow, 1994), by introducing the granular pressure and shear viscosity,

$$\left\langle \alpha\rho \vec{\boldsymbol{v}}^G \vec{\boldsymbol{v}}^G \right\rangle = \left\langle P^G \mathbf{I} - \mu^G \mathbf{D} \right\rangle \ , \qquad (13)$$

where $\mathbf{I}$ is the identity matrix and $\mathbf{D}$ is the strain rate tensor. The granular pressure is defined as

$$P^G = \alpha\rho\theta\left[1 + 2\left(1+e\right)\alpha g\right] \ , \qquad (14)$$

where e is the coefficient of restitution, accounting for inelastic collisions, and the radial distribution function is given by $g = 1\big/\left(1-\left(\alpha/\alpha_{\max}\right)^3\right)$. The second order term in α ensures that the maximum volume fraction, set to 65%, is not exceeded. The granular viscosity is defined by

$$\mu^G \equiv \alpha\rho\tau_c\theta \quad . \tag{15}$$

Assuming that production and dissipation balance, and neglecting fluid and compression effects, we model the collisional time-scale by

$$\tau_c^2 - \frac{3}{t_p S^2}\tau_c - \frac{3\left(1-e^2\right)}{4S^2} = 0 \quad , \tag{16}$$

where $S = \partial v_x/\partial y$. The granular temperature is given by

$$\theta = 3l^2/2\tau_c^2 \quad , \tag{17}$$

where the mean free path is the smaller of the average particle-particle and particle-wall distances, $l = \min\left\{d\sqrt[3]{\pi/6\alpha},\ y-d/2\right\}$.

Turbulence modeling

We employ the turbulence model, for the kinematic eddy viscosity, $\nu_{t,l}$, and the fluid rms velocity, $u_y^{+\prime\prime}$, of Johansen (1991a);

$$\nu_{t,l}^+ = \frac{\nu_{t,l}}{\nu_l} = \begin{cases} \left(y^+/11.15\right)^3 & \text{for } y^+ < 3.0 \\ \left(y^+/11.4\right)^2 - 0.049774 & \text{for } 3.0 \le y^+ \le 52.108 \\ 0.4y^+ & \text{for } 52.108 < y^+ \end{cases} \tag{18}$$

$$\sqrt{\left\langle u_y^{+\prime\prime}u_y^{+\prime\prime}\right\rangle} = \begin{cases} 0.033y^+\left[1-\exp\left(-\dfrac{y^+}{3.837}\right)\right]\exp\left(-\dfrac{\left(y^+/30.0\right)^{7.82}}{7.82}\right) & \text{for } y^+ \le 30.0 \\ u_y^{+\prime\prime}\left(30.0\right) & \text{for } y^+ > 30.0 \end{cases} \tag{19}$$

NEAR-WALL MODEL

Close to the wall, the flow regime is radically different from that of the bulk, and we may, because of this, impose several simplifying assumptions on the governing equations, in addition to those already mentioned. We will assume a boundary layer situation where there are two principal directions, x (parallel to the wall) and y (normal to and pointing away from the wall). We limit the study to low particle deposition rates, so it will be assumed that axial gradients are negligible, such that $\partial/\partial x \approx 0$, for all quantities. We furthermore assume that the particle velocity normal to the wall is negligible outside the boundary layer, at $y = y_{bulk} >> d/2$, and we get, by integrating Eq. (1) from $y = d/2$ to y_{bulk}, the steady particle deposition flux;

$$\frac{J_{y,wall}}{y_{bulk}} \approx -\frac{\partial}{\partial y}\left(\rho\alpha v_y\right) \quad . \tag{20}$$

Moreover, we assume that the liquid velocity normal to the wall is negligible in the boundary layer.

Adding up the axial components of the momentum equations, Eqs. (2) and (3), averaging over turbulent fluctuations, neglecting the inertial terms and assuming that the x-directional particle and liquid velocities only differ by a constant terminal velocity, we get the axial mixture momentum equation,

$$1 = \left[1 + \frac{\nu_t^+\rho_{mix}}{\rho_l} + \frac{\mu^G}{\mu_l}\right]\frac{\partial u_x^+}{\partial y^+} \quad , \tag{21}$$

where we have introduced the dimensionless velocity, $u_x^+ = u_x/u_\tau$, distance, $y^+ = \left(y-d/2\right)u_\tau/\nu_l$, and turbulent kinematic viscosity, $\nu_t^+ = \nu_t/\nu_l$. The mixture density is defined as $\rho_{mix} \equiv \alpha\rho + \alpha_l\rho_l$, and we have assumed that the particle turbulent viscosity can be approximated by the liquid turbulent viscosity.

The normal-to-wall particle velocity may be explicitly obtained from the y component of Eq. (3) and expressed as the sum of a convective drift velocity and a diffusive velocity;

$$v_y^+\Gamma = A^+ - \frac{B^+}{\alpha^+}\frac{\partial\alpha^+}{\partial y^+} \quad , \tag{22}$$

where we have ensemble averaged over turbulent realizations, and $\Gamma = 1 + \left(t_p^+/\alpha^+v_y^+\right)\partial\left(\alpha^+v_y^{+2}\right)/\partial y^+$. For stability reasons, we approximate $\Gamma \approx 1$, which is appropriate except in the XDLVO-dominated sub-layer close to the wall. The effective convective drift velocity is given by

$$A^+ = t_p^+\left[\underbrace{-\frac{1}{t_p^+}\frac{\beta_T}{T^+ + T_0^+}\frac{\partial T^+}{\partial y^+}}_{\text{Thermophoresis}} \underbrace{- \frac{\tau_L^+}{\tau_L^+ + t_p^+}\frac{\partial\left\langle u_y^{\prime\prime+2}\right\rangle}{\partial y^+}}_{\text{Turbophoresis}}\right. \\ \left. \underbrace{+\frac{3.08\mu_l}{u_\tau\rho d_p}\sqrt{\left|\frac{\partial u_x^+}{\partial y^+}\right|}\left(v_x^+ - u_x^+\right)}_{\text{Hydrodynamic lift}} + \underbrace{F_y^{XDLVO+}}_{\text{XDLVO forces}} - \underbrace{\frac{\partial P^{G+}}{\partial y^+}}_{\text{Granular pressure}}\right] \quad , \tag{23}$$

where the drift contribution of the thermal stress has been absorbed by the thermophoresis term. The granular pressure gradient will give both drift and diffusivity contributions, represented individually in Figs. 5 and 6 and, but kept as one term here. The effective diffusivity is expressed as

$$B^{+}=t_p^{+}\left[\underbrace{\frac{k_B q_{wall}}{\rho_l u_\tau^3 m_p C_{p,l}}\left(T^{+}+T_0^{+}\right)}_{\text{Brownian diffusivity}}+\underbrace{\frac{\left\langle u_y''^{+2}\right\rangle \tau_L^{+}}{\tau_L^{+}+t_p^{+}}}_{\text{Turbophoretic diffusivity}}+\underbrace{\frac{1}{t_p^{+}(1-\alpha)}\frac{\nu_t^{+}}{Sc_t}}_{\text{Turbulent diffusivity}}\right] \quad , \tag{24}$$

and we have introduced several dimensionless parameters and variables; $\alpha^{+}=\alpha/\alpha_{bulk}$, $t_p^{+}=t_p u_\tau^2/\nu_l$, $\rho_l^{+}=\rho_l/\rho$, $T^{+}=\left(T_l-T_{wall}\right)u_\tau\rho_l C_{p,l}/q_{wall}$, $T_0^{+}=u_\tau\rho_l C_{p,l}T_{wall}/q_{wall}$, $P^{G+}=P^{G}/\rho\alpha_{bulk}u_\tau^2$, and $F_y^{XDLVO+}=F_y^{XDLVO}6\nu_l/\pi d_p^3\rho u_\tau^3$. Combining Eqs. (22) and (20) we may express the dimensionless wall flux, $J_{wall}^{+}=J_{wall}/u_\tau\rho\alpha_{bulk}$, as

$$-\frac{J_{wall}^{+}}{y_{bulk}^{+}} = \frac{\partial}{\partial y^{+}}\left[\Gamma^{-1}\alpha^{+}A^{+}-\Gamma^{-1}B^{+}\frac{\partial\alpha^{+}}{\partial y^{+}}\right] \ . \tag{25}$$

Introducing turbulence, ensemble averaging, and adding the two energy equations Eqs. (5) and (6), assuming identical particle and liquid temperatures , we get

$$-\Pr=\left[1+k_h^{G+}+k_{h,t,l}^{+}+k_{h,t,p}^{+}\right]\ \frac{\partial T^{+}}{\partial y^{+}} \quad , \tag{26}$$

where the dimensionless heat conductivities are defined by $k_h^{+}=k_h/k_{h,l}$. We let the turbulent liquid and particle heat conductivities be defined as $k_{h,t,l}\equiv C_{p,l}\alpha_l\rho_l\nu_{t,l}/\Pr_{t,l}$, and $k_{h,t,p}\equiv C_{p,p}\alpha\rho\nu_t/\Pr_{t,p}$, and the granular heat conductivity is $k_h^{G}\equiv-\alpha k_{h,l}-C_{p,p}\alpha\rho v_y T+C_{p,p}\alpha\rho\nu_g/\Pr_{g,p}$. The turbulent liquid heat conductivity improves the liquid heat transport because of the mixing processes generated by the turbulent fluctuations. The over-all heat conductivity is modified by the presence of the particle phase, and the granular and turbulent particle heat conductivities give this contribution. The granular heat conductivity contains a reduction in the liquid heat conductivity due to the reduced liquid volume fraction, a convective particle heat transport contribution, and a contribution accounting for heat exchange between colliding particles. For low deposition rates, it is reasonable to neglect the convective particle heat transport. The turbulent particle heat conductivity accounts for the additional heat transport by turbulent particle fluctuations.

Boundary Conditions

Equation (25) needs boundary conditions at the wall and at the position y_{bulk} , whereas Eqs. (21) and (26) require boundary conditions at the wall. We apply the following boundary conditions;

$$\alpha\left(y=d/2\right)=0 \quad , \tag{27}$$

$$u_x(y=d/2)=0 \quad , \tag{28}$$

$$T_l(y=0)=T_w \quad , \tag{29}$$

$$\alpha\left(y=y_{bulk}\right)=\alpha_{bulk} \quad , \tag{30}$$

$$u_x(y=y_{bulk})=u_{x,bulk} \quad , \tag{31}$$

$$v_y(y=y_{bulk})=0 \quad , \tag{32}$$

$$T_l(y=y_{bulk})=T_{bulk} \quad . \tag{33}$$

NUMERICAL SOLUTION ALGORITHM

The system of equations, Eq. (21), Eq. (25) and Eq. (26), are solved numerically, for u_x^{+} , α^{+} and T^{+} , on a discrete grid, by applying the boundary conditions Eqs. (27) to (33). The grid extends from $y_1=d/2+h_0$ to $y_{1000}=0.01m$, where the grid point distances, y_j-y_{j-1} , increase logarithmically, and cell interfaces are put half-way between neighboring grid points. The equations are solved iteratively employing the following algorithm:

1. Initialize v_y^{+} , u_x^{+} , α^{+} and T^{+} and pick an initial guess for J_{wall}^{+} , u_τ and q_{wall} .
2. Solve for u_x^{+} , α^{+} and T^{+} .
3. Calculate J_{wall}^{+} and update u_τ , q_{wall} , v_y^{+} and θ^{+} .
4. Check if the correction of the calculated volume fraction profile is larger than some convergence criteria. If not converged return to step 2.
5. The solution is converged, and the final dimensionless mass transfer coefficient is J_{wall}^{+} .

RESULTS AND DISCUSSION

In this section we summarize some of the results we have obtained with the model described in this paper. We study the effect of the various physical phenomena, including turbulence, thermophoresis, granular pressure and XDLVO near-wall forces, and we study how particles of different diameters experience the various forces.

We define a base case using a bulk liquid velocity of 5 m/s, a wall temperature of $380\,K$ and a bulk temperature of $330\,K$. The bulk particle volume fraction is 20%, and the particle diameter is $1\,\mu m$. We use water heat conductivity $\left(0.6\ W/m\,K\right)$, specific heat capacity $\left(4180\ J/kg\,K\right)$, mass density $\left(1000\ kg/m^3\right)$, and viscosity $\left(1\cdot10^{-3}\ Pa\,s\right)$, for the liquid phase. The particle heat conductivity is $1\ W/m\,K$, the specific heat capacity is $1000\ J/kg\,K$, and the mass density is $2000\ kg/m^3$. We assume that the particles retain 50% of their kinetic energy after collisions, $e=0.5$. Turbulent Prandtl and Schmidt numbers are conveniently set to 1. In addition to the base case particle size we plot curves for particle diameters of $0.1\ \mu m$, $5\ \mu m$ and $10\ \mu m$.

As is shown in Fig. 2, the base-case model reproduces the typical deposition rate versus particle relaxation time plot (Johansen, 1991a; Guha, 2008). The base-case model includes Brownian diffusion, turbulence and hydrodynamic lift only. The effects of including granular pressure, thermophoresis and near wall XDLVO forces are also shown. Since the particle relaxation time depends on the particle diameter, Fig. 2 gives an impression of the particle size im pact on the deposition rate. Small relaxation times represent

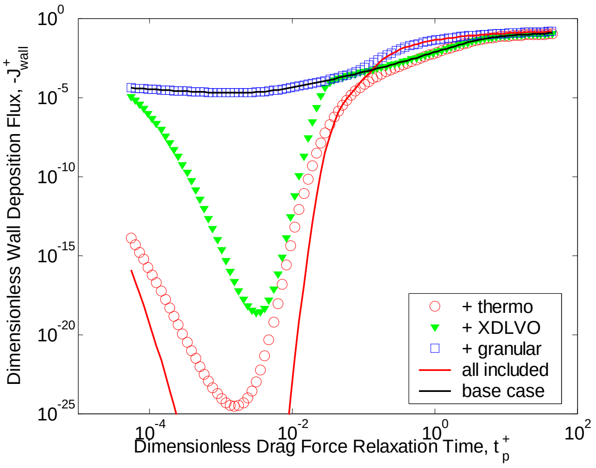

Fig. 2 The dimensionless wall-flux as a function of dimensionless particle relaxation time. Large diameters correspond to large t_p^+. The base-case includes Brownian diffusion, turbulence and lift only, while the other curves show the effect of including thermophoresis, XDLVO forces and granular stress, respectively.

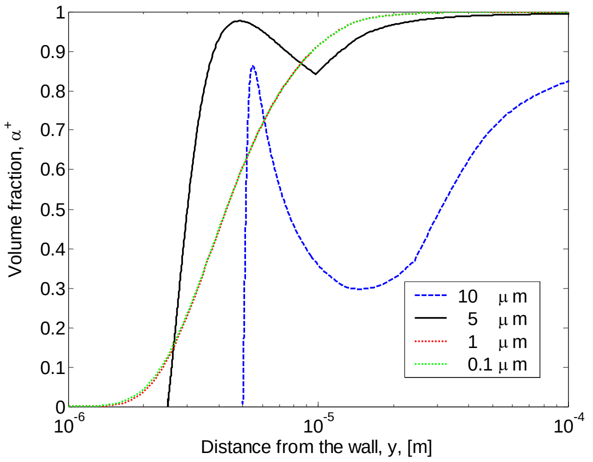

Fig. 3 Dimensionless volume fraction as a function of the wall distance; comparison of different particle sizes.

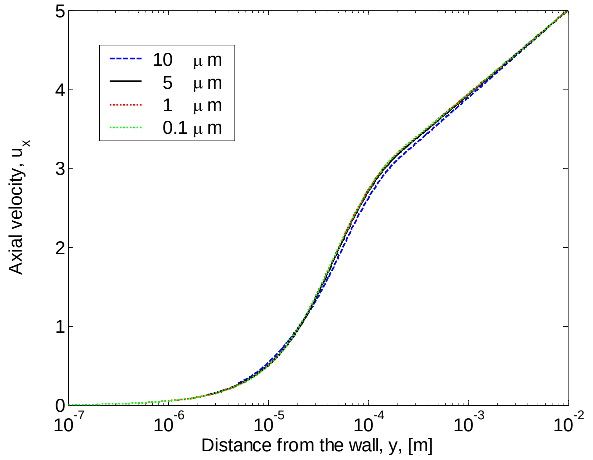

Fig. 4 Dimensionless axial liquid velocity as a function of the wall distance; effect of different particle sizes.

small particles and larger ones represent larger particles. The four particle sizes mentioned above correspond to relaxation times of $t_p^+ = 1\cdot 10^{-4}$, $5.5\cdot 10^{-3}$, $1.4\cdot 10^{-1}$ and $6\cdot 10^{-1}$, ordered by particle size. It is seen that for particles in the range $0.1-1\,\mu m$ extremely low deposition rates are to be expected. Repulsive thermophoretic and XDLVO forces result in strong reduction in this particle range. The granular stress increases the deposition rate, for large particles. Lift and gravity, not shown here, gave insignificant contributions.

In Fig. 3 the dimensionless particle volume fractions obtained for the four different particle sizes are compared. It is seen that the small particle volume fraction profiles are identical, while the larger particles' volume fractions show qualitatively quite a different behavior. This is due to the increased effect of turbophoresis, throwing the particles towards the wall. Repulsive forces restrict the deposition rate, so that a particle bank builds up close to the wall.

In Fig. 4 we see that the liquid velocities are not significantly altered by the particle size. Similarly, the temperature profiles are close to identical for the different particle sizes.

In Fig. 5 and 6, respectively, the base-case particle absolute values of the dimensionless drift velocity and diffusivity are plotted as functions of the wall distance. Note that when there are distinct dips in the profiles the sign has been changed between negative and positive in the log plot. All the contributions, shown in Eqs. (23) and (24), are included in the plots to show their relative importance in the over-all picture.

In Fig. 7 the base-case particle absolute value drift and diffusive velocities, as given by Eq. (22), are shown. It can be seen that the drift and diffusive velocities are almost equal, in magnitude, cancelling out each other, giving a disappearing particle velocity. The thermophoretic and EL contributions give rise to positive particle velocities, which contradicts the model assumption of negative particle velocities everywhere. This implies that no fouling occurs for this particle size. Close to the wall the negative drift velocity, due to attractive XDLVO forces (LW+AB), dominates, while the EL force gives a positive drift velocity from $y^+ \approx 4\cdot 10^{-4}$. From $y^+ \approx 3\cdot 10^{-2}$ thermophoresis is the dominating mechanism, being gradually evened out by turbulent dispersion. In the interval $y^+ \approx 10-30$ turbophoresis kicks in, giving a negative velocity.

For smaller particles, it can be shown that the diffusive term becomes more important, and in the inner XDLVO sub layer Brownian diffusion and XDLVO forces dominate.

For large particles, turbulent dispersion overwhelms the Brownian diffusion altogether, and turbophoresis is in magnitude, comparable to the thermophoresis. In addition, the granular pressure gradient becomes more important for larger particles. In the intermediate t_p^+ range of Fig. 2, where the wall flux goes from low to high, we go from a Brownian diffusion/thermophoresis dominated deposition regime to a situation where turbulence is dominating, and granular pressure controlled effects become important.

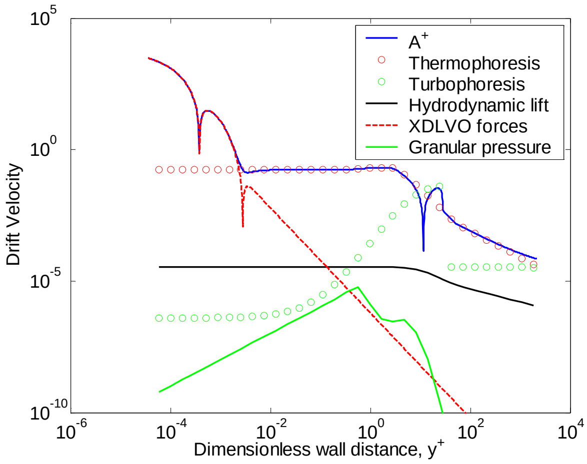

Fig. 5 Dimensionless drift velocity, A^+, and the different terms contributing (absolute values) as functions of the dimensionless wall distance, for 1 μm particles.

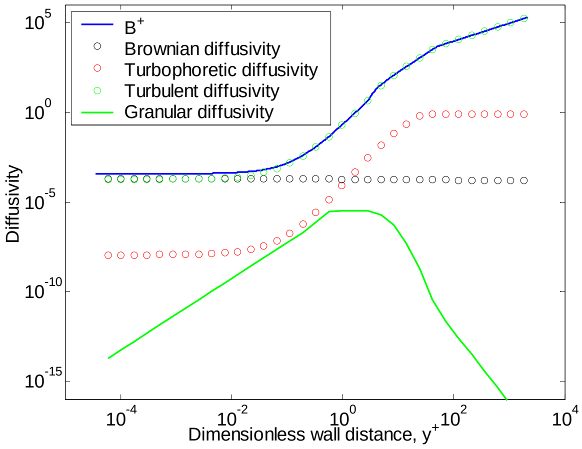

Fig. 6 Dimensionless diffusivity, B^+, and the different terms contributing (absolute values) as functions of the dimensionless wall distance, for 1 μm particles.

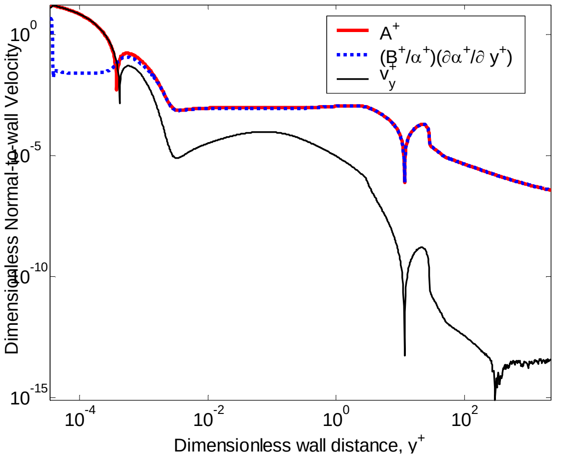

Fig. 7 Dimensionless drift and diffusive velocities and the normal-to-wall particle velocity, as given by Eq.(22), as functions of the dimensionless wall distance, for 1 μm particles.

CONCLUSIONS

A one-dimensional model has been developed for particle transport in the turbulent boundary-layer, including Brownian diffusion, thermophoresis, XDLVO near-wall forces and granular stress. The model can be employed to calculate mass-transfer coefficients for the particle phase, and may hence be implemented as a mass transfer boundary wall-function for coarse grid CFD simulations. The model shows that close to the wall XDLVO forces dominate, and repulsive XDLVO forces may prevent fouling by providing a repulsive buffer layer. The model indicates that also thermophoresis may prevent fouling effectively. The model furthermore shows that particles of different sizes may experience very different deposition mechanisms.

ACKNOWLEDGMENTS

This work was a part of the FOULSURFACE project which was carried out in MATERA ERA-Net cooperation between VTT Technical Research Centre of Finland, University of Oulu, SINTEF and University College Dublin. The project is jointly funded by Tekes, The Research Council of Norway, Enterprise Ireland, VTT, SINTEF and seven industrial companies from Finland, Sweden and Austria. The authors thank the research partners and funding organizations.

NOMENCLATURE

A	Total drift velocity, m/s .
A_H	Hamaker constant, *dimensionless*.
B	Total diffusion coefficient, m^2/s .
C_L	Lift coefficient, *dimensionless.*
C_p	Specific heat capacity, $J/kg\,K$.
d	Diameter, m .
$\mathbf{D}$	Strain rate tensor, $1/s$.
e	Granular coefficient of restitution, *dimensionless*.
$\hat{\mathbf{e}}$	Unit vector, *dimensionless*.
$\overline{\boldsymbol{f}}$	Force vector per unit volume, N/m^3 .
$\overline{\mathbf{F}}$	Force vector, N .
F_a	Faraday's constant, $96485\ C/mol$.
g	Radial distribution function, *dimensionless*.
$\overline{\boldsymbol{g}}$	Gravity, m/s^2 .
G	Gibbs free energy, J/mol .
h_0	Minimum separation due to Born repulsion, $0.158\ nm$.
h	Particle-wall separation, m .
$h_{p,l}$	Particle-liquid heat transfer coefficient, W/m^2K .
I	Ion strength, mol/m^3 .
$\mathbf{I}$	Identity matrix, *dimensionless.*
J	Mass flux, kg/m^2s .
k_B	The Boltzmann constant, $1.3807\cdot 10^{-23}\ J/K$.
k_h	Heat conductivity, $W/m\,K$.
k_m	Mass transfer coefficient, m/s .
l	Mean free path, m .

m	Particle mass, kg .
P	Pressure, Pa .
Pr	Prandtl number, *dimensionless*.
q	Heat flux, W/m^2 .
R	The universal gas constant, $8.314\,J/mol\,K$.
Sc	Schmidt number, *dimensionless*.
S	Strain rate, $1/s$.
t_p	Particle drag force relaxation time, s .
T	Temperature, K .
u_τ	Shear velocity, m/s .
$\vec{\mathbf{u}}$	Liquid velocity vector, m/s .
$\vec{\mathbf{v}}$	Particle velocity vector, m/s .
x	Cartesian coordinate, parallel to the wall, m .
y	Cartesian coordinate, normal to and pointing away from the wall, m .
α	Volume fraction, m^3/m^3 .
β_T	Thermophoretic force strength, *dimensionless*.
$\gamma^\pm$	Electron acceptor/donor surface energy, J/m^2 .
γ^{LW}	Lifshitz-van der Waals surface energy, J/m^2 .
ε	Dielectric permittivity, $C/m\,J$.
ζ	Electrical surface (zeta) potential, V .
θ	Granular temperature, m^2/s^2 .
κ	The inverse Debye screening length, $1/m$.
λ	The acid-base decay length, m .
μ	Dynamic viscosity, $Pa\,s$.
ν	Kinematic viscosity, m^2/s .
ρ	Mass density, kg/m^3 .
τ_c	Inter particle collision time-scale, s .
τ_L	Lagrangian time-scale, s .
$\boldsymbol{\tau}$	Shear stress tensor, Pa .

Subscripts

$_{bulk}$	Value outside the boundary layer.
$_{l,p,w}$	Property of the liquid, particle, wall.
$_{g,t}$	Granular, turbulent contribution.
$_{wall}$	Value at the wall.

Superscripts

$^+$	Dimensionless variable.
^{AB,EL,LW}	XDLVO acid-base, electrostatic and Lifshitz-van der Waals contributions.
^{G}	Granular collisional contribution.
^{R}	Random contribution.
^{S}	Soret (thermophoretic) contribution.
^{T}	Thermal contribution.
^{XDLVO}	Extended DLVO theory contribution.

Averaging

$<\ >$	Expectation value due to ensemble averaging.
$''$	Fluctuation about an ensemble averaged value.

REFERENCES

Adomeit, P. and U. Renz, 1996, Deposition of Fine Particles from a Turbulent Liquid Flow: Experiments and Numerical Predictions, *Chemical Engineering Science*, Vol 51, pp. 3491-3503.

Crowe, C. et al., 1997, *Multiphase flows with droplets and particles*, CRC Press, Boca Raton, Florida, USA.

Gidaspow, D., 1994, *Multiphase flow and fluidization*, Academic Press, San Diego, California, USA.

Guha, A., 2008, Transport and Deposition of Particles in Turbulent and Laminar Flow, *Annular Review of Fluid Mechanics*, Vol 40, pp. 311-341.

Hoek, E.M.V. and G.K. Agarwal, 2006, Extended DLVO interactions between spherical particles and rough surfaces, *Journal of Colloid and Interface Science*, Vol 298, pp. 50-58.

Johansen, S.T., 1991a, The Deposition of Particles on Vertical Walls, *International Journal of Multiphase Flow*, Vol 17, pp. 355-376.

Johansen, S.T., 1991b, Thermal inertial deposition of particles, *Proceedings of the International Conference of Multiphase Flows '91 Tsukuba*, Vol. 1, pp. 415-421.

McNab, G.S. and A. Meisen, 1973, Thermophoresis in Liquids, *Journal of Colloid and Interface Science*, Vol. 44.

Ojaniemi, U., et al., 2008, CFD Model for Particulate Fouling - Modeling Particle Adhesion on Surface with XDLVO Theory, *6th International Conference on CFD in Oil & Gas, Metallurgical and Process Industries*, SINTEF/NTNU, Trondheim, Norway.

Sippola M.R. and W.W. Nazaroff, 2002, Particle deposition from turbulent flow: Review of published research and its applicability to ventilation ducts in commercial buildings. Lawrence Berkeley National Laboratory, LBNL-(51432), Berkeley, CA.

Soo, S.L., 1989, *Particulates and continuum: multiphase fluid dynamics*, Hemisphere Publishing Corporation, New York, USA.

van Oss, C.J., 2006, *Interfacial forces in aqueous media*, CRC Press, Boca Raton, Florida, USA.

Wu W. et al., 1996, Change in surface properties of solids caused by grinding, *Powder Technology*, Vol. 89, pp. 129-132.